Development and initial evaluation of a dynamic species-resolved model for gas phase chemistry and size-resolved gas/particle partitioning associated with secondary organic aerosol formation

Robert J. Griffin

Institute for the Study of Earth, Oceans, and Space and Department of Earth Sciences, University of New Hampshire, Durham, New Hampshire, USA

Donald Dabdub

Department of Mechanical and Aerospace Engineering, University of California, Irvine, California, USA

John H. Seinfeld

Departments of Chemical Engineering and Environmental Science and Engineering, California Institute of Technology, Pasadena, California, USA

Received 20 July 2004; revised 26 October 2004; accepted 21 December 2004; published 15 March 2005.

[1] A module for predicting the dynamic evolution of the gas phase species and the aerosol size and composition distribution during formation of secondary organic aerosol (SOA) is presented. The module is based on the inorganic gas-aerosol equilibrium model Simulating the Composition of Atmospheric Particles at Equilibrium 2 (SCAPE2) and updated versions of the lumped Caltech Atmospheric Chemistry Mechanism (CACM) and the Model to Predict the Multiphase Partitioning of Organics (MPMPO). The aerosol phase generally consists of an organic phase and an aqueous phase containing dissolved inorganic and organic components. Simulations are presented in which a single salt (either dry or aqueous), a volatile organic compound, and oxides of nitrogen undergo photo-oxidation to form SOA. Predicted SOA mass yields for classes of aromatic and biogenic hydrocarbons exhibit the proper qualitative behavior when compared to laboratory chamber data. Inasmuch as it is currently not possible to represent explicitly aerosol phase chemistry involving condensed products of gas phase oxidation, the present model can be viewed as the most detailed SOA formation model available yet will undergo continued improvement in the future.

Citation: Griffin, R. J., D. Dabdub, and J. H. Seinfeld (2005), Development and initial evaluation of a dynamic species-resolved model for gas phase chemistry and size-resolved gas/particle partitioning associated with secondary organic aerosol formation, *J. Geophys. Res.*, *110*, D05304, doi:10.1029/2004JD005219.

1. Introduction

[2] A significant fraction of atmospheric organic aerosol is formed through in situ oxidation of volatile organic compounds (VOCs) followed by partitioning of low-volatility products into the aerosol phase. This component of atmospheric organic aerosol is referred to as secondary organic aerosol (SOA). In order to produce an accurate estimate of the climatic and urban pollution effects of SOA, it is necessary to understand and model the molecular mechanisms of SOA formation and how these mechanisms are influenced by atmospheric conditions such as temperature, relative humidity (RH), and the presence of other constituents in the aerosol. Atmospheric VOCs (generally those containing five or more carbon atoms) that produce SOA include aromatics, alkenes, alkanes, and certain oxygenated hydrocarbons that are emitted from both biogenic and anthropogenic sources.

[3] The gas phase oxidation chemistry of SOA-forming VOCs is complex and not fully understood. The gas-to-particle conversion step in the formation of SOA is the partitioning of the semivolatile or nonvolatile products of VOC oxidation between the gas and particle phases. Chemical analysis of the SOA identifies many products that condense, thereby allowing formulation of gas phase pathways that potentially lead to those products [*Yu et al.*, 1999]. The ambient atmospheric particulate matter (PM) into which this partitioning occurs consists, in general, of a mixture of organic and inorganic components, including water, and itself may consist of one or more phases; if more than one phase exists, it has been presumed in general that one of the phases is primarily an organic phase and the other is predominantly an aqueous phase [*Seinfeld and Pankow*, 2003].

Copyright 2005 by the American Geophysical Union.
0148-0227/05/2004JD005219

[4] The formation of SOA from a particular VOC is often described in terms of the fractional mass yield, Y, which relates how much PM is produced when a certain amount of parent gaseous VOC is oxidized, $Y = M_o/\Delta\mathrm{VOC}$, where M_o ($\mu g\ m^{-3}$) is the mass concentration of SOA produced from the reaction of ΔVOC ($\mu g\ m^{-3}$). *Odum et al.* [1996] developed an empirical framework for representing the functional dependence of Y on M_o for chamber experiments. Assuming that the photo-oxidation of a parent VOC leads to just two overall semivolatile products, P_1 and P_2, that are representative of the overall product mixture, then

$$\text{(R1)} \qquad \mathrm{VOC} + \mathrm{oxidant} \rightarrow p_1\mathrm{P}_1 + p_2\mathrm{P}_2$$

where p_1 and p_2 are molar stoichiometric coefficients. Reaction (R1) is not likely to represent a fundamental reaction because of its empirical derivation. Mass-based stoichiometric factors for the production of P_1 and P_2 from the parent hydrocarbon are then defined as $\alpha_1 = p_1 \times \mathrm{MW}_{\mathrm{P}_1}/\mathrm{MW}_{\mathrm{VOC}}$ and $\alpha_2 = p_2 \times \mathrm{MW}_{\mathrm{P}_2}/\mathrm{MW}_{\mathrm{VOC}}$ where MW represents molecular weight [*Seinfeld and Pankow*, 2003]. The empirical two-product representation of SOA formation has been highly successful in fitting laboratory SOA yield data for dozens of parent VOCs, and it serves as the basis for estimating SOA formation in current global models [*Chung and Seinfeld*, 2002; *Tsigaridis and Kanakidou*, 2003; *Lack et al.*, 2004].

[5] Even though its simplicity and its firm basis in actual laboratory data are strong points, this approach has limitations for use in atmospheric models. It is well established that, even for a single VOC, many more than two products are involved in SOA formation and, as conditions such as temperature, RH, and oxidant level vary, the functionality and phase distribution of condensing products are likely to change [see, e.g., *Forstner et al.*, 1997; *Yu et al.*, 1999; *Jaoui and Kamens*, 2003; *Gao et al.*, 2004]. A major need in atmospheric modeling of SOA is to formulate models that are based more explicitly on actual chemistry, both gas and aerosol phase, but that are also constrained by observed laboratory data. Furthermore, such models need to minimize computational demand.

[6] The approach to modeling the gas phase chemistry associated with SOA formation that is, in principle, most chemically rigorous is to represent the gas phase chemistry with a fully explicit mechanism, an example of which is the University of Leeds Master Chemical Mechanism version 3.0 (http://www.chem.leeds.ac.uk/Atmospheric/MCM/main.html#Master) [*Jenkin et al.*, 2003; *Saunders et al.*, 2003]. Even though many of the rate constants and branching ratios have to be estimated, the use of such a mechanism allows explicit prediction of each of the condensing products. The concentrations of the condensing products predicted explicitly can then be used to predict SOA formation by considering the thermodynamic properties of the products [*Jenkin*, 2004]. Nevertheless, the computational demand associated with using a fully explicit mechanism in a regional or global atmospheric model render it impractical.

[7] Regional- or global-scale gas phase chemistry is typically represented by lumped mechanisms, those in which reactions of similar type are grouped together or in which the chemistry of certain species is used to represent that of a wide spectrum of related compounds. Approaches based on lumped mechanisms are starting to emerge in regional/global modeling of SOA [e.g., *Griffin et al.*, 2002a, 2002b], and it is this direction that offers the most promise for development of chemically explicit models of SOA formation that are, at the same time, computationally feasible for global models.

[8] Until recently, the accepted picture of SOA formation was that no further chemistry occurs in the aerosol phase once the oxidation products condense. Two major discoveries have altered this view. First, it was discovered that particle phase acidity increases SOA formation beyond that under less acid conditions [*Jang and Kamens*, 2001; *Jang et al.*, 2002; *Czoschke et al.*, 2003; *Iinuma et al.*, 2004]. Second, the presence of oligomeric species was discovered in the SOA aerosol phase [*Limbeck et al.*, 2003; *Gao et al.*, 2004; *Iinuma et al.*, 2004; *Kalberer et al.*, 2004; *Tolocka et al.*, 2004]. Such oligomers have been identified as SOA constituents in both the presence and absence of acidic seed aerosols [*Gao et al.*, 2004; *Kalberer et al.*, 2004]. In terms of aerosol phase chemistry, no models currently exist that describe these reactions, even at the laboratory level, because of a lack of understanding of what reactions occur and the kinetic and thermodynamic properties to describe the hypothesized processes [*Barsanti and Pankow*, 2004].

[9] It is of interest, both in analyzing laboratory chamber data and in simulating atmospheric particle evolution resulting from condensation of organic species, to be able to simulate the evolution of the aerosol composition and size distribution during SOA formation. Chamber studies on SOA formation generally produce time-dependent aerosol size distributions that evolve as the semivolatile and nonvolatile products of VOC oxidation condense onto existing inorganic seed particles or nucleate to form new particles. These size distributions then serve as the basis on which the yield of SOA from a particular VOC is determined [see, e.g., *Cocker et al.*, 2001]. At moderate and high values of RH, the chamber seed aerosol contains water as well, affecting the gas-particle partitioning (as well as the particle phase chemistry) of gas phase VOC oxidation products, so that it is necessary to account for the presence of both liquid water and a condensed organic phase in the aerosol.

[10] A fundamental approach to predict SOA formation is to couple a chemical mechanism that represents the gas phase chemistry of the parent VOCs to a module that describes the condensation of semivolatile and nonvolatile oxidation products [see, e.g., *Jacobson*, 1997; *Meng et al.*, 1998; *Griffin et al.*, 2002a, 2002b, 2003; *Pun et al.*, 2002, 2003]. A comprehensive model of the evolution of the aerosol composition and size allows one to evaluate, through comparison with laboratory data, the extent to which the entire mechanism of gas-to-particle conversion is understood. The model also allows one to predict, on first principles, the effect on the amount of organic aerosol formed of variables such as temperature, RH, VOC chemical structure and initial mixing ratio, and the inorganic composition of the aerosol. Eventually, such a model must include particle phase chemistry. At this point in time, however, while the existence of particle phase chemistry has been demonstrated clearly, it is not possible to attempt to represent that chemistry explicitly.

[11] In this work, a model for size- and composition-resolved SOA formation is presented and applied in a systematic series of numerical experiments to examine SOA formation, as might be performed in a series of experiments in a laboratory chamber. The goal of this model is to serve both as a vehicle for quantitative analysis of aerosol data in chamber experiments on SOA yields and chemistry and as a predictive model to be embedded in three-dimensional atmospheric models. We begin with a description of the basic model, which has evolved based on previous work of *Meng et al.* [1998], *Griffin et al.* [2002a, 2002b, 2003], *Nguyen and Dabdub* [2002], and *Pun et al.* [2002]. We then discuss the treatment of inorganic/organic aerosol thermodynamics because the gas-aerosol equilibrium state is that which drives the gas-to-particle conversion. A number of case studies are considered to illustrate the predicted behavior of SOA formation from different parent VOCs, based on current representation of gas phase oxidation products and the associated thermodynamics. At present we compare only the qualitative behavior of the model with actual laboratory experiments to assess the ability to capture the main features of SOA formation. The model is formulated in such a manner as to allow improvements in representation of gas or aerosol phase processes, especially aerosol phase chemistry, to be included and to allow implementation of the modules into three-dimensional atmospheric models.

2. Model Description

2.1. Inorganic Aerosol

[12] The model for the dynamics of the size composition distribution of the inorganic aerosol is based on the particle mass distribution as a function of particle diameter, D_p. The mass-conservative approach solves the aerosol condensation/evaporation equation [*Pilinis*, 1990; *Meng et al.*, 1998; *Griffin et al.*, 2002b]. The aerosol condensation/evaporation equation is solved using the partitioned flux integrated semi-Lagrangian method (PFISLM) of *Nguyen and Dabdub* [2002]. This routine is mass (though not number) conservative, positive definite, and peak retentive and has been applied in previous three-dimensional model simulations of ambient PM formation [*Griffin et al.*, 2002b]. Such a treatment of inorganic aerosols allows for dynamic calculations that do not rely on the assumption of instantaneous equilibrium.

[13] When both neutral and ionic PM species are present in the solution, the thermodynamics of the system is complex because of (1) the effects of ions on the activity coefficients of neutral species and on those of other ions, (2) the change of ion solvation shells with composition, (3) the effects of neutral species on the activity coefficients of ions, (4) the acid-base and ion pair formation equilibria, and (5) the consideration of electroneutrality [*Pankow*, 2003]. Currently, general techniques do not account for all of these issues in mixed inorganic/organic systems, although work is ongoing in that direction for specific aerosol constituents [*Clegg et al.*, 2001, 2003; *Ming and Russell*, 2002; *Clegg and Seinfeld*, 2004; *Erdakos et al.*, 2005]. Several existing inorganic gas-aerosol thermodynamic models are capable of predicting the gas-aerosol phase distribution of components such as ammonia, nitric acid (HNO_3), hydrochloric acid, sulfuric acid, and water with consideration of nonvolatile inorganic cations such as sodium, magnesium, potassium, and calcium. (See *Zhang et al.* [2000] for a review of such models.) The routine Simulating the Composition of Atmospheric Particles at Equilibrium 2 (SCAPE2) [*Kim et al.*, 1993; *Meng et al.*, 1995, 1998] is used in the present model to calculate surface vapor pressures for inorganic species. While SCAPE2 is chosen for this study, the techniques used allow for adaptation and use of any inorganic aerosol model.

2.2. Organic Aerosol Equilibrium

[14] Because of the complex nature of the mixture of species in atmospheric particles, it is highly possible that more than one condensed phase is present in an individual particle. When two liquid phases coexist in an atmospheric particle, one may be predominantly an aqueous phase with some dissolved organic material, and the other a largely organic phase with a small water concentration [*Seinfeld et al.*, 2001; *Pankow*, 2003]. With multiple phases, each dissolved species attempts to distribute itself among the gas phase and the condensed phases in such a way as to achieve the overall thermodynamic equilibrium that is attained when the chemical potential of each species is identical in each of the phases. Two condensed liquid phases can arise when both hydrophilic and hydrophobic organic compounds are present. Atmospheric oxidation of VOCs produces polar compounds that tend to be hydrophilic, whereas primary anthropogenic and biogenic PM organics tend to be hydrophobic. However, these hydrophobic primary organic PM species provide a medium into which polar compounds potentially are absorbed.

[15] Models have been developed to predict the gas-aerosol phase distribution of organic compounds and water to form a single organic plus water PM phase [*Pankow et al.*, 2001; *Seinfeld et al.*, 2001; *Seinfeld and Pankow*, 2003]. The UNIFAC model [*Fredenslund et al.*, 1977] has proven useful for computing liquid phase activity coefficients of such organic plus water solutions, as well as for estimating pure compound vapor pressures of organic species [*Asher et al.*, 2002]. The most general version of the organic plus water condensed phase model developed to date is the Model to Predict the Multiphase Partitioning of Organics (MPMPO) [*Griffin et al.*, 2003], in which particles are assumed a priori to be one of two types (a purely organic aerosol or an aqueous aerosol with associated molecular and ionic components) or to have two separate phases, one primarily aqueous and the other predominantly organic. Equilibrium is computed for all species among the gas phase and the two condensed phases. Models do not yet exist that automatically compute the number of condensed phases based entirely on overall thermodynamic phase equilibrium for all species, but work is proceeding in that direction [*Pankow*, 2003]. In the model of *Griffin et al.* [2003], equilibrium between the gas and particulate phases is assumed for organic species. The aerosol condensation/evaporation equation expresses how the entire aerosol size distribution evolves dynamically toward an equilibrium state (and thus is a more general statement of the gas-aerosol partitioning process), but this equation is solved only for inorganic aerosol constituents.

[16] In the current work, an adapted version of the gas phase Caltech Atmospheric Chemistry Mechanism (CACM) [*Griffin et al.*, 2002a] is used to simulate gas phase chemistry leading to formation of semivolatile and nonvolatile organic oxidation products. The predictions from CACM are used in conjunction with an updated version of MPMPO [*Griffin et al.*, 2003] to compute the equilibrium relationship between dissolved organic components in both aqueous and organic condensed phases and their atmospheric gas phase concentrations. Detailed improvements to the CACM and MPMPO modules are described subsequently. The MPMPO utilizes the following equilibrium relationships. The equilibrium organic aerosol phase mass concentration of an individual species i, O_i ($\mu g\ m^{-3}$ air), is given by the following relationship:

$$O_i = K_{om,i} G_i M_o = \frac{G_i M_o RT}{M_{om} 10^6 \gamma_i p^o_{L,i}} \quad (1)$$

$K_{om,i}$ (m^3 air μg^{-1}) is the partitioning coefficient that describes the phase distribution of the condensing organic species [*Pankow*, 1994], G_i is its corresponding gas phase concentration ($\mu g\ m^{-3}$ air), and M_o is the total concentration ($\mu g\ m^{-3}$ air) of organic aerosol mass available to act as the partitioning medium. R is the ideal gas constant (8.2×10^{-5} m^3 atm mol^{-1} K^{-1}), T is temperature (K), M_{om} is the average molecular weight (g mol^{-1}) of the absorbing organics including both primary and secondary organic compounds, $p^o_{L,i}$ is the pure component vapor pressure (atm) of species i, and γ_i is the activity coefficient of species i in the organic phase. The factor of 10^6 converts g to μg.

[17] If A_i represents the aqueous phase concentration of species i ($\mu g\ m^{-3}$ air) and H_i its Henry's law coefficient (($\mu g\ \mu g^{-1}$ H_2O)/($\mu g\ m^{-3}$ air)), A_i is given by:

$$A_i = \frac{G_i(\mathrm{LWC})H_i}{\gamma_{aq,i}} \quad (2)$$

where LWC is the aerosol liquid water content (μg H_2O m^{-3} air) and $\gamma_{aq,i}$ is the activity coefficient of organic species i in the aqueous phase normalized by that at infinite dilution. The aqueous phase equilibrium is subject to constraints imposed by dissociation of the dissolved organic species, if applicable, which necessitates knowledge of the aqueous phase pH [*Griffin et al.*, 2003]. In addition, as shown in equations (1) and (2), both the organic and aqueous phase equilibria require activity coefficients. The UNIFAC method is employed to determine the activity coefficients in both types of phases. When equations (1) and (2) are combined with a mass balance for each of the partitioning species (i.e., the total mass concentration of a species predicted by the chemical mechanism must equal the sum of its concentrations in all of the phases), the result is a series of n equations and n unknowns that is solved iteratively using the techniques described by *Griffin et al.* [2003] to determine the phase distribution of semivolatile organic species formed via VOC oxidation.

[18] It must be stressed that the aerosol condensation/evaporation equation is applied to inorganic aerosol species and equations (1) and (2) are applied to organic aerosol species. The two sets of equations are linked as follows. Over the course of the aerosol model time step, the condensation/evaporation equation is applied to partitioning inorganic aerosol species such as sulfate and nitrate. At the end of the aerosol time step, SCAPE2 has predicted the phase distribution of inorganic aerosol species, the LWC of the aerosol, and the pH of the aqueous phase. At this point, the bulk equilibrium associated with equations (1) and (2) is applied to organic species; this application requires both the LWC and the pH predicted by SCAPE2. Uptake of additional water is considered for any organics that partition to the aqueous phase. If this amount of water is insignificant (less than one percent of the LWC associated with the inorganic aerosol), the aerosol calculation for the current time step is complete. However, if the amount of additional water associated with the organics is significant, the aerosol module returns to the beginning of its time step and runs SCAPE2 while considering both the aqueous organic material and the additional water. This iterative process is repeated until the LWC of the aerosol is consistent between SCAPE2 and MPMPO.

[19] The calculations associated with MPMPO are not performed in a particle-size-dependent manner. Preexisting organic PM and LWC are summed across all size bins to provide a bulk state of the aerosol to use with the equilibrium partitioning equations. The total mass of each SOA constituent in the aerosol phase is found from application of MPMPO, and this mass is spread between bins based on available particle surface area for particles smaller than 2.5 μm in diameter. This weighting procedure is based on the preexisting mass in each bin being converted to a particle number and that particle number concentration being used to estimate available surface area in each bin. The fraction of SOA partitioned to a bin is equal to the fraction that the preexisting particles in the bin contribute to the total available surface area. Total mass is then redistributed amongst bins based on whether the added (or removed) mass would cause a particle to grow (or shrink) to sizes outside of the original bin width. This is clearly a simplified method of accounting for changes in particle size due to formation of SOA, especially because the dynamic inorganic and bulk equilibrium organic modules are linked through the LWC. Future work will be directed toward combining the PFISLM and MPMPO modules such that the condensation/evaporation equation can be applied to perform size-resolved simulations of SOA formation. It should also be noted that the LWC or preexisting organic aerosol mass concentrations could be used as the basis for the weighted distribution of SOA mass. However, the surface area is chosen because the LWC and preexisting organic aerosol mass are summed in the application of equations (1) and (2) to provide a bulk equilibrium condition. Therefore a variable independent of LWC and preexisting organic aerosol mass is desired.

2.3. Updates to Previous Versions of the Models

[20] *Pun et al.* [2003] outline uncertainties associated with the model predictions of SOA concentrations using this approach and the differences that result when these predictions are compared to predictions from other methods that are based on parameters derived primarily from chamber experiments. These differences are linked to

Table 1. Changes Made to the Original Version of the CACM During This Work[a]

Change	Reaction Numbers	Adaptations Made	Reasons/Notes
1	(79)	increase yield of $RO_2$21 to 0.1 and decrease that of RAD3 to 0.74	Increasing the yield of $RO_2$21 enhances the formation of ring-retaining products. This causes simulations to be in line with observations of *Forstner et al.* [1997] and AROL to be consistent with other aromatic parent species.
2	(97)–(109)	increase RAD reaction rate constants with NO_2 by a factor of 1.7 and adjust those with O_2 by a factor of 0.9	These changes also enhance the formation of ring-retaining products.
3	(128), (136), (156), (269), (284), (298), (306), (315), (329), (345)	decrease rate constants of acyl peroxy radical reactions with HO_2 by a factor of 3.5	At low VOC and NO_x levels in the original versions of the modules, acyl radical consumption is dominated by reaction with hydroperoxy radicals, leading to acid products. This generates high SOA yields in cases with low initial VOC concentrations, behavior not observed in laboratory chamber experiments [*Odum et al.*, 1996, 1997a, 1997b; *Hoffmann et al.*, 1997; *Griffin et al.*, 1999].
4	(197)–(202)	decrease yield of species UR7 to 0.3 and add formation of species UR10 at a yield of 0.7[b]	In the initial development of the model it was assumed that UR7 would not contribute significantly to SOA due to its relatively high vapor pressure. However, its formation in high yield and its lumping into a less volatile surrogate lead to overpredictions of SOA. UR10 is not a partitioning species in the model.
5	(221), (228), (242), (249), (256)	increase reaction rate by 20%	Faster isomerization of benzyl peroxy radicals leads to increased formation of anhydride and furan type products to be more in line with the results of *Forstner et al.* [1997].
6	(222)–(224), (229)–(231), (243)–(245), (250)–(252)	decrease yield of species RPR9 (or its corresponding product, RP11, RP12, or RP13, in the latter sets of reactions) to 0.3 and add formation of a new species (UR35) at a yield of 0.7	In the initial development of the model it was assumed that RPR9 (or its corresponding product in the latter sets of reactions) would not contribute significantly to SOA due to its relatively high vapor pressure. However, its formation in high yield and its lumping into a less volatile surrogate lead to overpredictions of SOA. UR35 is not a partitioning species in the model.
7	(235)	increase reaction rate by 10%	Faster isomerization of benzyl peroxy radicals leads to increased formation of anhydride and furan type products to be more in line with the results of *Forstner et al.* [1997]. A slower isomerization rate in this case relative to those listed above is one pathway by which AROH leads to higher yields of SOA than does AROL.
8	(236)–(238)	decrease yield of species RP11 to 0.5 and add formation of UR35 at a yield of 0.5	In the initial development of the model it was assumed that RP11 would not contribute significantly to SOA due to its relatively high vapor pressure. However, its formation in high yield and its subsequent formation of UR26 lead to overpredictions of SOA. In this case, 0.5 is used (as opposed to the 0.3 used above for RPR9) to provide another pathway by which AROH leads to higher yields of SOA than does AROL.
9	(334)	decrease the yield of UR26 to 0.67 and add the formation of UR24 at a yield of 0.33	UR26 is a major constituent of SOA from aromatic ring degradation products, which was originally simulated to be too high. UR24 is not a partitioning species in the model.
10	(350)–(361)	treat highly functionalized alkyl nitrate (AP) products as unreactive species (set k_{350} through $k_{361} = 0$)	Structure-activity-relationship-based rate coefficients lead to rapid consumption of the AP products, leading to a peak followed by a decline in SOA concentrations in model simulations. No such peaks have been observed in chamber experiments [*Odum et al.*, 1996, 1997a, 1997b; *Hoffmann et al.*, 1997; *Griffin et al.*, 1999].

[a]Reaction numbers and product designations refer to those presented by *Griffin et al.* [2002a].
[b]In reaction (197) these values need to be multiplied by CF(28).

disparities in modeled partitioning and stoichiometric coefficients of the semivolatile organic compounds (SVOCs) predicted to constitute SOA. This provides motivation to investigate the formation chemistry and properties of SVOCs in the models presently discussed. As a result, the original CACM and MPMPO were revised and applied to simulate numerous atmospherically relevant scenarios.

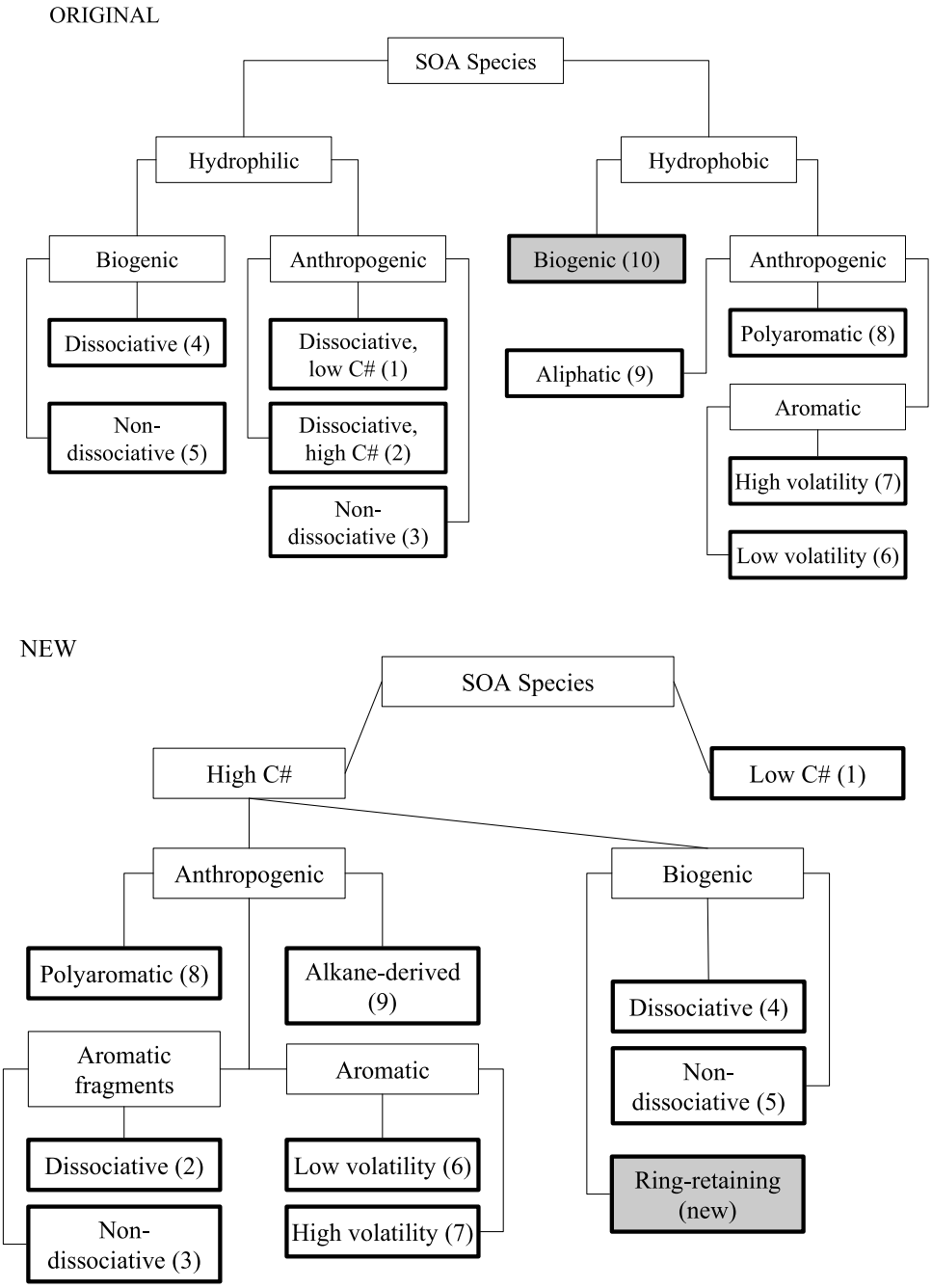

Figure 1. Lumping of SOA surrogate species (top) in previous studies [*Pun et al.*, 2002; *Griffin et al.*, 2003] versus (bottom) that used in this study. Numbers correspond to structures given by *Griffin et al.* [2003]. Shading indicates that a required change in surrogate structure was needed; bold outlining represents the end of the branches in the classification.

2.3.1. Updates to CACM

[21] A summary of the changes made to CACM reactions and the motivations behind them are presented in Table 1. Reaction numbers included in Table 1 correspond directly to those listed by *Griffin et al.* [2002a]; in the following discussion, indices describing changes refer to the first column in Table 1. Of the 10 changes included in Table 1, seven (changes 1, 2, and 5–9) affect only the aromatic chemistry and are made to achieve better agreement between simulations and observed product distributions [*Forstner et al.*, 1997] and to provide a greater distinction between aromatic compounds with high and low SOA yields (AROH and AROL, respectively) as defined by *Odum et al.* [1997a]. Correspondingly, only one change (change 4) affects solely the chemistry of biogenic compounds (to compensate for overprediction of SOA formation); the remaining two (changes 3 and 10) are more general changes that affect both aromatic and biogenic

chemistry and that are implemented to match the temporal behavior in simulations more accurately to that observed in chamber experiments. All ten of these changes are focused primarily on adjustment of estimated stoichiometric factors and kinetic reaction rate constants that inherently have some amount of associated uncertainty. Because of lack of chamber data to which simulated SOA formation could be compared, no changes have been made to the gas phase chemistry of long-chain alkanes and polycyclic aromatic hydrocarbons (PAH) in CACM. The chemistry of smaller VOCs also remains unchanged because such chemistry is much better understood and because, in the mechanism, it has very little influence on SOA formation. In addition, the chemical loss coefficient for species that are deemed nonreacting species in CACM [*Griffin et al.*, 2002a] is decreased from 10^{-3} to 10^{-4} min^{-1} in order to reflect more accurately the temporal profiles of SOA when particle deposition is taken into account in the chamber experiments for the simulations discussed below.

2.3.2. Updates to MPMPO

[22] In addition to changes being necessary in CACM, this work also provided the opportunity to revise the MPMPO module, as summarized in Table 2. In the following discussion, indices for changes refer to the first column in Table 2. The most significant changes made to the partitioning module are focused on the way in which secondary species capable of forming SOA are classified into surrogate groups. This lumping procedure was deemed necessary to reduce the computational demand of the partitioning code, especially when implemented into a three-dimensional air quality model. Figure 1 (top) indicates the original lumping procedure to determine surrogate structures. In the original model formulated by *Pun et al.* [2002], surrogate species are classified as being either hydrophobic or hydrophilic, based on an assumption as to whether partitioning to the aqueous or organic condensed phase dominates. In this earlier version of the partitioning module, species are forced to partition only to one phase or the other. Species are then classified by source (biogenic versus anthropogenic), structure, volatility, and potential for dissociation (in the case of hydrophilic species). *Griffin et al.* [2003] extended the original model of *Pun et al.* [2002] by allowing all surrogate species to partition to both the aqueous and condensed organic phases. In the current work, a distinction between hydrophobic and hydrophilic compounds is no longer made because all surrogates are allowed to partition to both phases (change 1). The result is the grouping shown in Figure 1 (bottom). The distinction for surrogate assignment is based on structure, source, volatility, and dissociative capabilities only. However, because of the original surrogate structures chosen, no changes in structure are required for nine of the ten groups in terms of the surrogate used. The biogenic, ring-retaining group is new (change 2) and is assigned the structure 1-methyl-1-hydroxy-2-nitrato-4-isopropyl-cyclohexane. The molecular weight (217 g mol^{-1}) and vapor pressure (6.58×10^{-6} atm at 298 K, prior to the vapor pressure correction methodology described subsequently) of this species are introduced into the partitioning module in order to replace the original hydrophobic, biogenic category (group number 10 in Figure 1, top). Species included in the new group are AP7, AP8, UR5, and UR6 (changes 3 and 4). Ring fragmentation products originally classified as hydrophobic and biogenic are reclassified (changes 5 and 6) into the other biogenic categories (group numbers 4 and 5 in Figure 1, bottom). UR7 (originally in group number 10) is now considered a nondissociative biogenic ring fragmentation product (group number 5), and UR8 (also originally in group number 10) is now considered a dissociative biogenic ring fragmentation product (group number 4).

[23] Another change in the lumping procedure that is expected to alter the predictions of partitioning behavior is the switch from a hydrophobic, anthropogenic, aliphatic category (group number 9 in Figure 1, top) to an anthropogenic, alkane-based category. In the original classification, all but one of the partitioning species lumped into this category are derivatives of long-chain alkanes. One bifunctional ring fragmentation product of aromatic chemistry (UR26) is included; this species is not deemed hydrophilic based on the criteria described originally by *Pun et al.* [2002]. However, a long-chain alkane derivative is used as the surrogate for this group. These choices lead to overprediction of SOA formation from the aromatic compounds leading to this bifunctional species because the vapor pressure of the long-chain alkane surrogate is predicted to be considerably lower than that of the aromatic ring fragmentation product. This species has been removed from its original group (group number 9) and is now included with the dissociative aromatic fragments (group number 2 in Figure 1, bottom) (change 7). It should also be noted that products ARAC and UR19 are included in groups 7 and 8, respectively, though not specified by *Pun et al.* [2002].

[24] Under certain circumstances, products deemed capable of partitioning to the aerosol phase by the criteria of *Pun et al.* [2002] react quickly in the gas phase to form products further down the oxidation chain that are significantly more volatile and therefore assumed not to form SOA. For example, assume that gas phase product A is formed from the initial reaction between a VOC and an oxidant, that A is capable of forming SOA, and that the gas phase oxidation of species A leads to the formation of species B, which is not considered capable of forming SOA. Schematically, this is represented by:

$$\text{(R2)} \qquad \text{VOC} + \text{oxidant} \rightarrow \text{A} \leftrightarrow \text{SOA}$$

$$\text{(R3)} \qquad \text{A} + \text{oxidant} \rightarrow \text{B}$$

At earlier points in the oxidation of the parent VOC, A is present in significant concentrations, leading to SOA formation. However, as time increases, A remaining in the gas phase is converted to B, and the mass of A in the aerosol phase repartitions to the gas phase to reestablish equilibrium. Such behavior leads to a peak followed by a decline in SOA concentration in some simulations. This behavior has not been observed in the smog chamber experiments being simulated [*Odum et al.*, 1996, 1997a, 1997b; *Hoffmann et al.*, 1997; *Griffin et al.*, 1999]. Therefore highly reactive products, such as the hypothetical A, are assumed not to partition to the aerosol phase despite meeting the partitioning criteria originally outlined by *Pun et al.* [2002]. Aldehydic species that contain a ketone in the

Table 2. Changes Made to the Original Version of the MPMPO During This Work[a]

Change	Adaptations Made	Reasons/Notes
1	general reclassification of lumped surrogate groups	Hydrophobicity and hydrophilicity are no longer used as a means by which to group partitioning compounds. See Figure 1.
2	replacement of original group 10 with a ring-retaining biogenic category that has a different surrogate species	This adaptation is based on change 1.
3	remove AP7 from original group number 5 and move to the new ring-retaining biogenic group	This adaptation is based on change 2.
4	remove AP8, UR5, and UR6 from original group number 10 and move to the new ring-retaining biogenic group	These adaptations are based on change 2.
5	move UR7 from original group number 10 to the nondissociative biogenic ring-fragmentation product group (group number 5)	This adaptation is based on change 2.
6	move UR8 from original group number 10 to the dissociative biogenic ring-fragmentation product group (group number 4)	This adaptation is based on change 2.
7	move UR26 from the aliphatic anthropogenic hydrophobic group (original group 9) to the dissociative aromatic ring-fragmentation product group (group 2)	This adaptation is based on change 1 and also is made because UR26 is significantly more volatile than the other products in original group 9.
8	remove PAN8, RPR3, and RPR4 from consideration for partitioning	Inclusion of these species caused a temporal peak and subsequent decline in SOA simulations, which was not observed in the chamber experiments being simulated [*Odum et al.*, 1996, 1997a, 1997b; *Hoffmann et al.*, 1997; *Griffin et al.*, 1999].
9	remove UR22 from consideration for partitioning	The vapor pressure of this species was reevaluated using a structure-activity relationship and deemed too high to participate realistically in the partitioning process.
10	adjustment of vapor pressures of surrogate compounds	Vapor pressures were adjusted to avoid underprediction of SOA, to attempt to account for the effects of particle phase chemistry, and to match average vapor pressures estimated from the chamber experiments being simulated [*Odum et al.*, 1996, 1997a, 1997b; *Hoffmann et al.*, 1997; *Griffin et al.*, 1999].

[a]Product descriptions and group numbers refer to those presented by *Griffin et al.* [2002a, 2003], *Pun et al.* [2002], and Figure 1.

α position are examples of species that follow this type of behavior:

$$\text{(R4)}\qquad \mathrm{RC(O)C(O)H + OH\ or\ NO_3} \rightarrow \mathrm{RC(O)C(O)O_2\cdot} \rightarrow \mathrm{RC(O)O_2\cdot} \rightarrow \mathrm{RO_2\cdot}$$

where R is an organic group that may or may not contain functionality. In the first step, OH or NO_3 abstracts the aldehydic H atom. Oxygen quickly adds to the resulting radical to form the first acyl radical shown. In a NO_x-rich environment, the acyl radical converts NO to NO_2 and fragments to form carbon dioxide and a radical that again quickly adds oxygen to form a second acyl radical. This reaction sequence continues and forms a simple peroxy radical as shown in the last step. Therefore products with this type of functionality are capable of losing two carbon atoms and two functional groups relatively quickly, which leads to increases in vapor pressure and decreases in simulated SOA.

[25] As a result, PAN8 and RPR3 are no longer constituents of SOA (originally in group number 10 and group number 5, respectively), and RPR4 no longer contributes to the high-volatility aromatic group (group number 7) (change 8). In addition, UR22 is removed from the low-volatility aromatic group (group number 6) upon reevaluation of its vapor pressure estimated using structure activity techniques (change 9).

[26] The last change (change 10) made to the MPMPO in this work is an adjustment of the predicted vapor pressures of the partitioning surrogate compounds, which are likely to have significant associated uncertainties [*Hemming and Seinfeld*, 2001]. This is performed because simulations that exclude such adjustment but include the improvements to CACM and the MPMPO discussed so far significantly underpredict SOA formation relative to experimental data. Such simulations also show a lag in the initialization of SOA formation relative to that in experiments. As discussed above, the partitioning methodology presented here also does not account for particle phase chemistry leading to very low vapor pressure material in the organic aerosol phase, as hypothesized by *Jang et al.* [2002] and observed by *Kalberer et al.* [2004]. To account for these factors, the estimated vapor pressures of the surrogate compounds are adjusted.

[27] The first step in the adjustment procedure is to consider the partitioning coefficients of the oxidation products of aromatic and monoterpene precursor compounds determined by *Odum et al.* [1996, 1997a, 1997b], *Hoffmann et al.* [1997], and *Griffin et al.* [1999] using a two-product model to fit chamber data. Using an average temperature of 308K and assuming ideality ($\gamma_i = 1$) and an average molecular weight of 180 g mol^{-1} [*Pankow*, 1994], it is possible (using equation (1)) to derive vapor pressures for both hypothetical products of the two-product fit. Typically, the two products represent one of higher and one of lower volatility. The vapor pressures calculated in this way are averaged over all the individual aromatics or all the individual monoterpenes investigated experimentally to yield one effective average representative vapor pressure each for SOA from aromatics (4.4×10^{-8} atm) and monoterpenes (1.7×10^{-8} atm), respectively. For the surrogate species in MPMPO that result from aromatic oxidation, vapor pressures in the current model are adjusted such that the chamber-based average vapor pressure falls between those of the high- and low-volatility ring-retaining products shown in Figure 1 (bottom) (division by factors of 1.5 and 1.4, respectively, for group number 6 and group

number 7) and between those of the dissociative and nondissociative fragmentation products shown in Figure 1 (bottom) (no correction and division by a factor of 33.0, respectively, for group number 2 and group number 3). At the same time, the average of the vapor pressures of the four surrogate species needs to be approximately equal to the chamber-based average vapor pressure. A similar procedure is followed for dissociative and nondissociative ring fragmentation products of monoterpenes shown in Figure 1 (bottom) (division by factors of 3.3 and 15.0, respectively, for group number 4 and group number 5) relative to the average chamber-based vapor pressure for SOA from biogenics. In the case of the ring-retaining products (the new surrogate group shown in Figure 1, bottom), the structure-activity relationship results in a vapor pressure almost 400 times as large as the chamber-based average. Such a large correction should not be used, and a correction factor of 66.0 is used, as that is twice the largest correction used for aromatic compounds. The vapor pressure of the polyaromatic surrogate (group number 8) is decreased by a factor of 2.4 so that it is approximately half of that of the high-volatility aromatic organics, as the polyaromatic surrogate contains a higher number of carbon atoms but similar functionality. Without such a correction, PAH species form less SOA than corresponding monoaromatic compounds on a mass reacted basis. Without appropriate information, no changes are made to the vapor pressure estimates for the long-chain alkane derivative (group number 9). The vapor pressure of the short-chain oxidation product surrogate (group number 1) also remains unchanged as the estimated value is close to that measured experimentally. While similar vapor pressure adjustments have been made in previous simulations of chamber chemistry [*Colville and Griffin*, 2004], it must be stressed that this corrective approach needs to be performed with caution due to its inherent uncertainties. However, once it is possible to describe explicitly particle phase chemistry or currently unknown gas phase reactions that lead to additional nonvolatile products, the model vapor pressures will be returned to values estimated using the structure-activity relationship, and the model will be expanded to include particle phase chemistry and the additional gas phase reactions. At that point, the need to adjust surrogate product vapor pressures will be revisited.

3. Inorganic Aerosol Simulations

[28] Model performance is evaluated by simulating several case scenarios. First, several simulation runs focused on inorganic aerosols are performed in order to confirm that adapting CACM and MPMPO (thereby changing the structures and amounts of SOA partitioning to the aqueous phase) did not alter the ability of SCAPE2 to simulate inorganic aerosol dynamics. Predictions of deliquescence relative humidity (DRH) are generally within 1–2% of observations and are consistent across all of the salts tested. A simulation is also performed in which NO_x and a VOC that is not predicted to form SOA are exposed to deliquesced particles and light to initiate photochemistry. The photolysis rate constants are based on simulations of air quality in the South Coast Air Basin of California (SoCAB) and are scaled depending on solar zenith angle, vertical position in the atmosphere, and sky clarity [*McRae*, 1981; *Lurmann et al.*, 1987]. For this simulation, overhead sun is assumed, and a scaling factor of 1.0 is used to assume top of the boundary layer under clear sky, unpolluted conditions. The gas phase chemistry of the system leads to gas phase formation of HNO_3, which heterogeneously reacts with aqueous sodium chloride aerosol to lead to the displacement of chloride by nitrate in the aqueous phase, as has been observed to occur in aged sea-salt aerosol [*Gard et al.*, 1998]. Therefore updating CACM and MPMPO has not altered the ability of SCAPE2 to simulate dynamics of inorganic aerosol systems.

4. Secondary Organic Aerosol Simulations

[29] The primary goal of the model is to simulate SOA formation. We consider four individual parent hydrocarbons, AROL, AROH, and low- and high-yield monoterpenes (BIOL and BIOH, respectively), for which outdoor chamber data are available for comparison. Because of lack of experimental data, simulations of SOA from oxidation of long-chain alkanes and PAH are not considered here.

[30] An initial VOC to NO_x ratio of 5 ppb C ppb^{-1} and an initial NO to NO_2 ratio of 2 are used in all SOA simulations, unless otherwise noted. A photolysis parameter of 0.5 is used, which is more indicative of a surface value under polluted, cloud-free conditions in the SoCAB where the outdoor chamber experiments being simulated were performed. This photolysis parameter also results in average OH radical concentrations of approximately 10^6 molecules cm^{-3}, a value in agreement with that estimated by *Odum et al.* [1997a] for the outdoor chamber experiments. Constant temperature (308K) and RH (5%) are also assumed. The temperature used represents the approximate average temperature of the experiments described by *Odum et al.* [1996, 1997a, 1997b], *Hoffmann et al.* [1997], and *Griffin et al.* [1999]. At this RH, the ammonium sulfate seed particles are essentially dry. A particle number concentration of 10,000 cm^{-3} in the smallest model size bin (in this case, 0.056 μm in diameter) is assumed, simply as a basis for calculation of initial particle mass. Assuming a density of 1.2 g cm^{-3}, this equates to an approximate initial ammonium sulfate mass of 1.1 μg m^{-3}. The gas phase time step is determined internally by the stability of the differential equations that need to be solved. The aerosol module is called once every minute of model time. Total simulation time ranges from 6 to 14 hours, depending on the parent species; these simulation times are roughly equivalent to the duration of the experiments.

[31] Initial aromatic mixing ratios used range from 150 to 250 ppb, with simulations performed at each step of 10 ppb. The range used for monoterpenes is 100 to 200 ppb. For BIOL, a test of temperature sensitivity at a single mixing ratio (200 ppb) is performed to ensure that the model follows the expected temperature-dependent behavior of partitioning [*Sheehan and Bowman*, 2001; *Takekawa et al.*, 2003]. One case study in which RH is increased over the DRH of ammonium sulfate is also performed under the same base conditions. In each case, a short-chain alkene (1-pentene in CACM) is included at a mixing ratio of 300 ppb, to mimic the inclusion of propylene at similar levels in the experiments being simulated. An additional

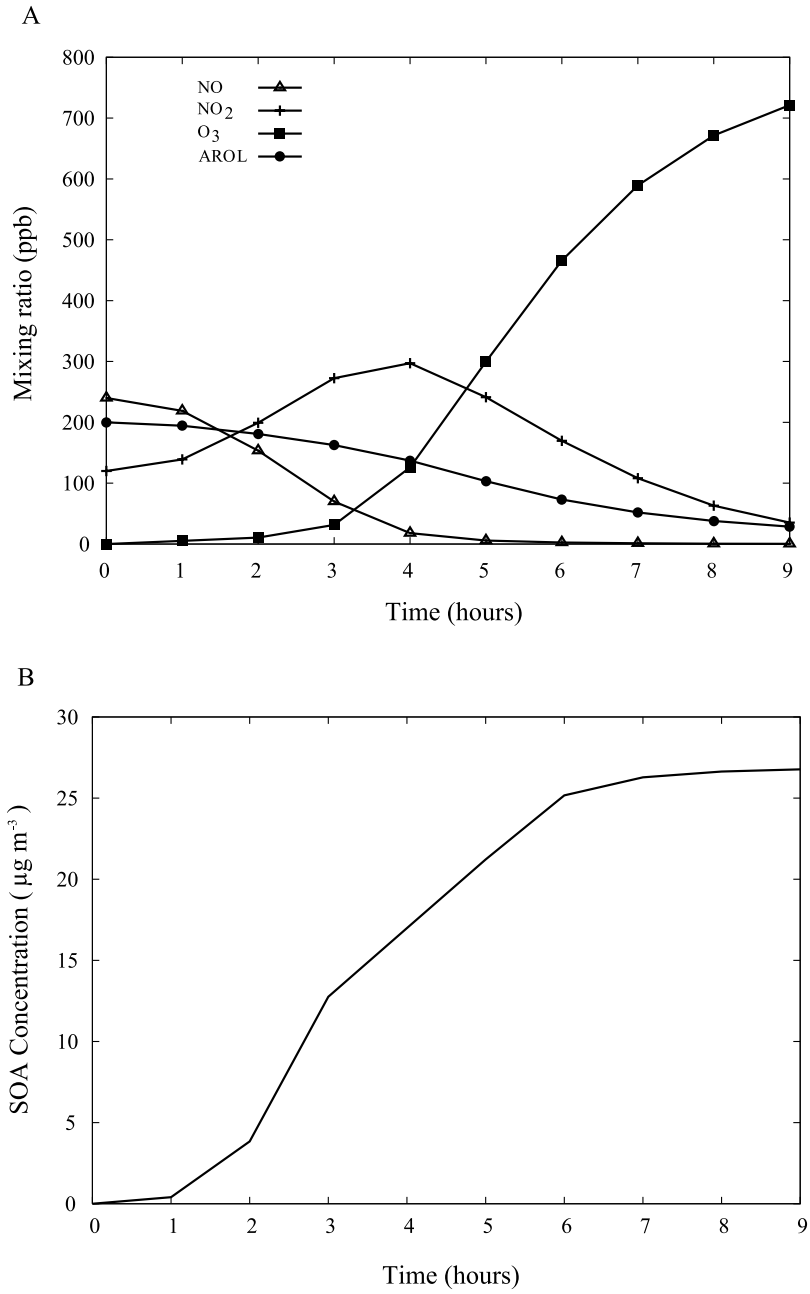

Figure 2. Predicted temporal profiles from photooxidation of 200 ppb AROL, 300 ppb of a short-chain alkene, 240 ppb NO, and 120 ppb NO_2 in the presence of 1.1 μg m^{-3} ammonium sulfate seed aerosol at 308 K and 5% RH. (a) Gas phase. (b) SOA.

simulation for the base case is performed in which the short-chain alkene is not included to investigate the impact of this compound on SOA yield, as discussed by *Takekawa et al.* [2003].

[32] Figures 2 and 3 show typical results from the simulations. For an initial AROL mixing ratio of 200 ppb, Figure 2a shows predicted temporal gas phase mixing ratios of AROL, NO, NO_2, and O_3, while Figure 2b indicates the predicted temporal mass concentration profile of SOA. These predictions qualitatively match the profiles obtained in the chamber experiments. The initial seed aerosol size distribution begins to grow after a lag at the beginning of the experiment. The SOA, which is the mass added to the initial seed particles, increases, eventually reaching a plateau. Figure 3 shows the simulated changes in aerosol size distribution throughout the course of the photo-oxidation. Initially, particles containing only ammonium and sulfate are present in the smallest size bin, as indicated by Figure 3 (top left). As time increases, ammonium, sulfate, and organics shift toward larger bins until the size distribution attains essentially constant behavior, which occurs after approximately 8 hours. This corresponds to a depletion of the AROL to such an extent that organic chemistry no longer contributes to additional particulate mass. Note that

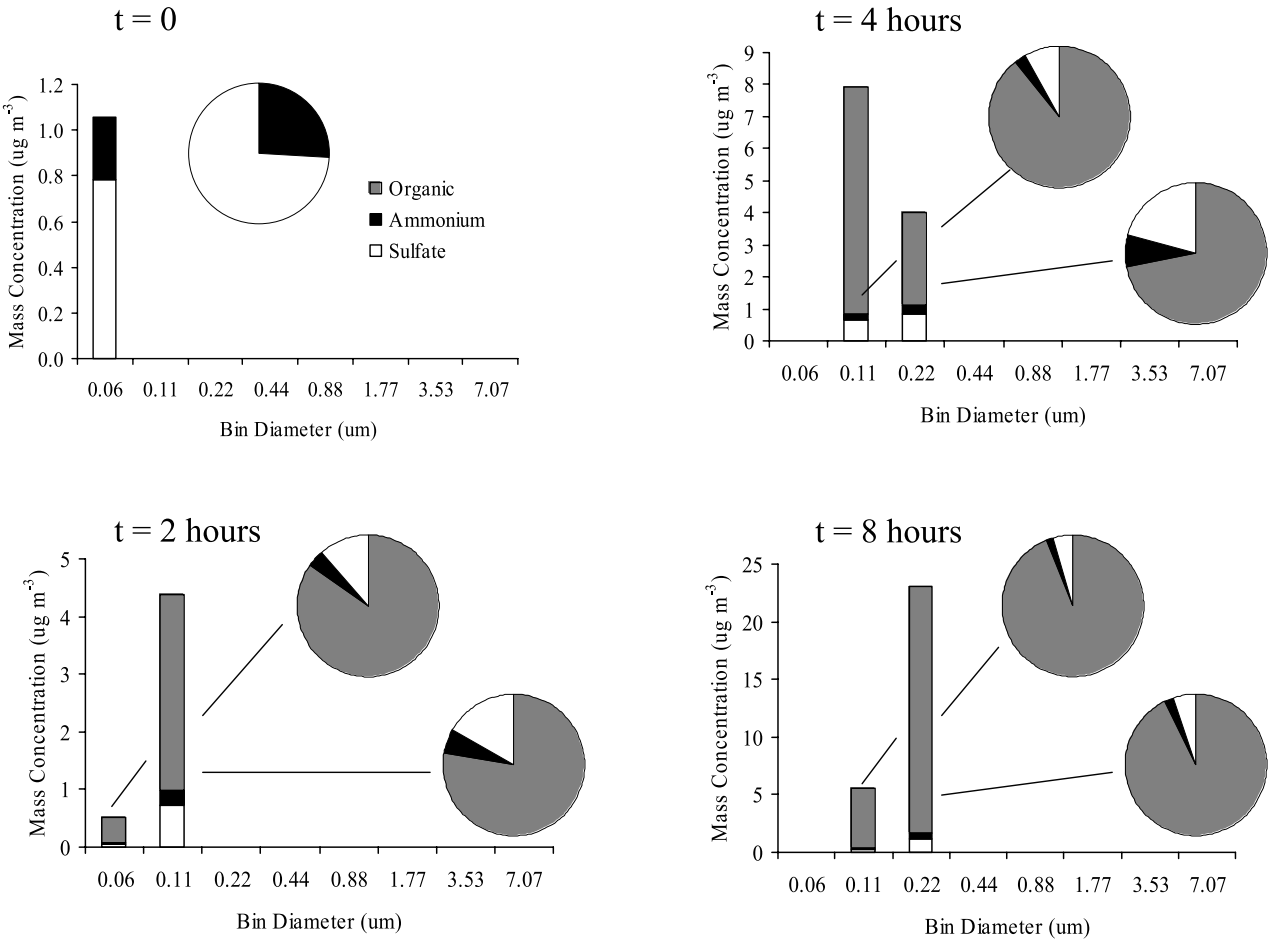

Figure 3. Distribution of aerosol phase species among particle size bins as a function of time for the simulation of Figure 2. Note that the scale of the ordinate changes with time. The contribution of each species on a percentage mass basis to each aerosol bin is also indicated.

the scale on the ordinate changes as simulation time increases from zero to eight hours. Figure 3 also indicates the percentage of the mass in each particle bin that is derived from the species present. Initially, only sulfate and ammonium contribute to aerosol mass. After 2 hours, organics contribute more than 80% of the particle mass in each bin. The mass-based particle size distribution shown in Figure 3 results from the simplified method used to predict changes in particle size due to bulk SOA formation, as discussed above. Future work will be directed toward more accurate predictions of mass-based particle size distributions that result from SOA formation by linking the MPMPO and PFISLM modules.

4.1. Aromatics

[33] Simulations with the aromatic parent VOCs are shown in Figure 4 as Y versus M_o, the manner in which experimental data commonly are displayed [*Odum et al.*, 1996, 1997a, 1997b; *Hoffmann et al.*, 1997; *Griffin et al.*, 1999]. Here, each value of Y and M_o is that at the end of an experiment, and discrete points represent individual model simulations as opposed to chamber data. We do not explore the predicted effect of NO_x level on SOA formation in aromatic systems here. In Figure 4, curves generated by a two-product model by *Odum et al.* [1997a] for AROL and AROH experiments are shown in addition to the simulation results. Simulation results are enveloped by the experimentally derived curves, indicating that, on average, simulation of SOA from oxidation of a mixture of AROL- and AROH-type species is in reasonable accord with observations. It should be noted that as initial parent hydrocarbon mixing ratios increase (and therefore ΔVOC increases because simulations are carried out until the parent hydrocarbon is consumed completely), both simulated Y and M_o values increase, as is expected based on gas-particle partitioning theory. The lowest initial mixing ratio is indicated by the simulation furthest to the left, and the highest by the furthest to the right. Increasing initial mixing ratios are indicated by the simulation points going from left to right. Oxidation of AROH also produces larger concentrations of SOA on the basis of mass of parent VOC reacted than oxidation of AROL does; this is most easily discerned at the high end of the simulation data, where three AROH simulations extend beyond the AROL simulation at the highest initial mixing ratio. It is also interesting that there is not much separation between the simulated SOA yields for AROL and AROH, despite AROH producing more partitioning

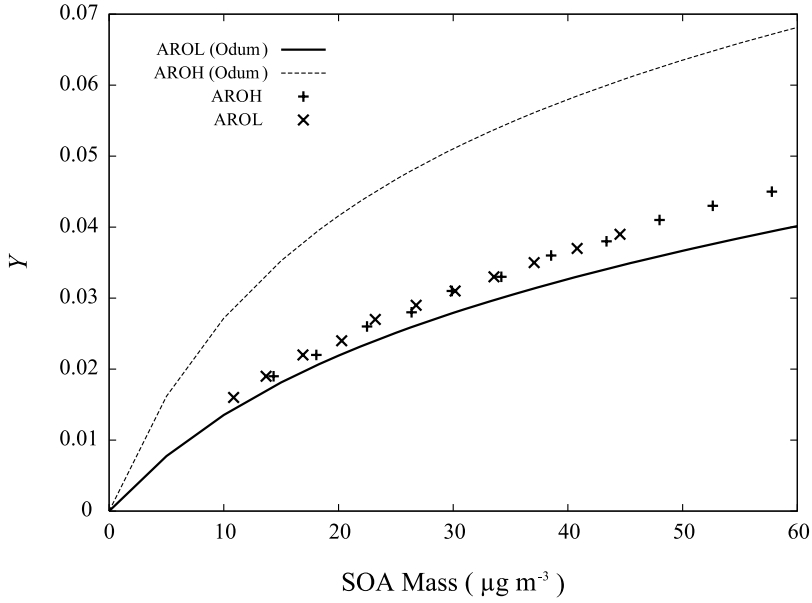

Figure 4. SOA yield versus organic aerosol mass concentration for aromatic species at 308 K and 5% RH. Individual simulations from the current work are designated by discrete points. Curves are based on experimental data of *Odum et al.* [1997a] and are derived using a two-product model. AROH are generally those aromatics with one or no methyl substituent groups; AROL conversely represents those with multiple methyl substituent groups. In CACM, AROL is represented by 1,2,3-trimethylbenzene and AROH by *n*-propyl-toluene.

mass stoichiometrically in the model than AROL does. This is a direct consequence of the lumping of partitioning species.

4.2. Monoterpenes

[34] Simulations of SOA formation from BIOL and BIOH are shown in Figure 5. In contrast to the data presented in Figure 4, the simulations for the monoterpenes are not enveloped by the experimentally derived curves. The simulated SOA formation for BIOL matches well the experimental curve fit for α-pinene, despite α-pinene not serving as the parent VOC structure; the simulations for BIOH fall between the two curve fits. This indicates that simulation of SOA formation from a mixture of monoterpenes would

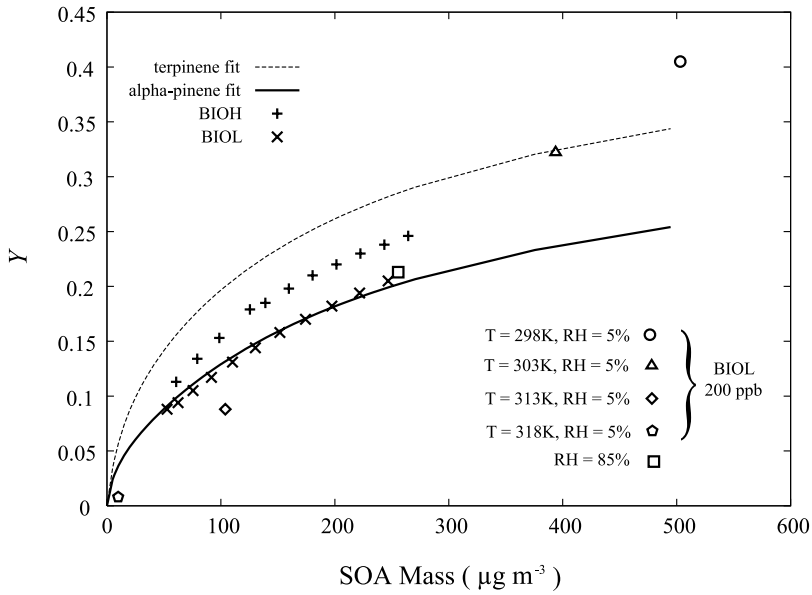

Figure 5. SOA yield versus organic aerosol mass concentration for biogenic species. Individual simulations from the current work are designated by discrete points. Curves are based on experimental data of *Odum et al.* [1996] (α-pinene, solid) and *Griffin et al.* [1999] (terpinenes, dashed) and are derived using a two-product model. In CACM, BIOL is represented by α-terpineol and BIOH by γ-terpinene.

likely underpredict total SOA formation. However, like the results presented in Figure 4, Y and M_o both increase as the initial mixing ratio (and therefore ΔVOC) of either BIOL or BIOH is increased. Lowest mixing ratios are on the left and highest on the right. Also similar to the results in Figure 4, on a per initial mixing ratio basis (assuming complete parent hydrocarbon consumption), oxidation of BIOH produces greater concentrations of SOA than does oxidation of BIOL. That is, for example, oxidation of 100 ppb of BIOL leads to a lower SOA concentration (52.8 $\mu g\ m^{-3}$) and yield (8.8%) than the corresponding oxidation of 100 ppb of BIOH (60.7 $\mu g\ m^{-3}$ and 11.3%, respectively, for SOA concentration and yield). In contrast to the results presented for aromatic precursor VOCs, a greater separation exists between the SOA yields for BIOL and BIOH. This occurs because oxidation of BIOH leads to greater formation of dissociative ring fragmentation products (group number 4), while BIOL leads to greater formation of the nondissociative ones (group number 5). The two compounds form stoichiometrically similar amounts of the newly included ring-retaining biogenic derivatives. Dissociative properties in this case result from carboxylic acid functional groups, which typically result in decreased vapor pressures relative to species containing nondissociative functional groups such as alcohols and carbonyls. Therefore BIOH yields greater SOA formation because it forms a larger amount of less volatile oxidation products.

[35] Data presented in Figure 5 also include the results from a short sensitivity evaluation using a base case condition of 200 ppb of BIOL. All other conditions are held constant, except as discussed below. The first variable investigated is temperature. Simulations are performed in which temperature is increased and decreased by 5 and 10K. As expected on the basis of the work of *Sheehan and Bowman* [2001], higher temperatures lead to decreased gas-particle partitioning, whereas lower temperatures increase SOA concentrations and yields. This is a direct result of the explicit and implicit (through the dependence of vapor pressure) effect of temperature on the partitioning coefficient (equation (1)). Temperature changes of this magnitude are not predicted to alter significantly the simulation of gas phase chemistry.

[36] One additional simulation is performed in which the RH is increased to 85%, which is above the DRH of the ammonium sulfate seed particles. This experiment is performed at 308K with an initial BIOL mixing ratio of 200 ppb and all other conditions as given previously. In this scenario, SOA forms either by formation of a new organic condensed phase or absorption into the aqueous phase because both aqueous and organic phases are assumed to exist when liquid water is present in the particle. The simulation predicts little change of SOA yield from the case in which dry seed aerosol is present under identical conditions. While little change in total SOA concentration is predicted, the presence of the aqueous phase potentially changes the way that SOA mass is distributed between the organic and the aqueous condensed phases. The model of *Griffin et al.* [2003], which is the precursor to that presented here, predicts increasing partitioning to the aqueous phase with increased LWC. However, in the case of the scenario in which RH is increased to 85% in the current model, it is estimated that over 95% of the SOA resides in an organic phase, with the remainder residing in an aqueous phase. The potential reason for the difference between the current and previous work is the smaller LWC that results in this model as a result of the use of SCAPE2; the work presented by *Griffin et al.* [2003] set a relatively large LWC as an input parameter. In addition, significantly higher organic precursor concentrations are used in this study; these concentration levels promote partitioning to an organic-only phase. Future versions of the model that more accurately reflect the interactions between organic and inorganic material in the particle, particularly in the aqueous phase, may reveal changes in SOA concentration and composition caused by variation of the composition and state of the inorganic seed aerosol used in chamber experiments [*Gao et al.*, 2004].

[37] An additional sensitivity case was simulated using the base case conditions without the short-chain alkene in an effort to match the observation of *Takekawa et al.* [2003] that indicated that the presence of the short-chain alkene enhances SOA yield. The study of *Takekawa et al.* [2003] compared two sets of experiments performed with similar α-pinene levels but in different chamber systems. The sensitivity run produced here is unable to match these results. A slight increase (less than 10%) in SOA production is observed in the base case scenario without addition of the short-chain alkene. This increase is traced to an increase in the level of ring-retaining products, the bulk of which are derived from OH-NO_x chemistry. *Colville and Griffin* [2004] also indicate the importance of such compounds in chamber studies of SOA formation from monoterpenes. The absence of the alkene leads to a decrease in predicted O_3 level, which leaves greater opportunity for the parent hydrocarbon to be consumed by OH, a process less likely to lead to ring fragmentation when compared to O_3-initiated oxidation. Clearly, there is a gap in understanding the gas or particle phase chemistry occurring in systems in which short-chain alkenes are included, despite the current gas phase chemical mechanism incorporating the most up-to-date scientific information. It is recommended that additional studies investigating the impact of the presence of short-chain alkenes on SOA yield be performed.

5. Discussion and Conclusions

[38] Prediction of SOA yield and speciation is challenging because of the vast number of potential participating species, as well as general uncertainties regarding the gas phase chemistry that leads to the formation of condensable species, the gas-particle partitioning process, and the occurrence of particle phase chemistry. Allowing adjustment of product vapor pressures in lieu of a direct treatment of particle phase chemistry, the features of SOA formation in chamber experiments are, on the whole, well matched for aromatic and biogenic VOCs using the updated modules discussed here.

[39] Relative to previous applications, the decreases in vapor pressure that have been incorporated into MPMPO will lead to increases in predicted SOA formation, while the relumping procedure and adjustments to stoichiometric coefficients and rate constants (particularly for acyl chemistry at low initial parent mixing ratios) that have been made will lead to decreases in predicted SOA formation. With respect to application to the SoCAB, the relumping

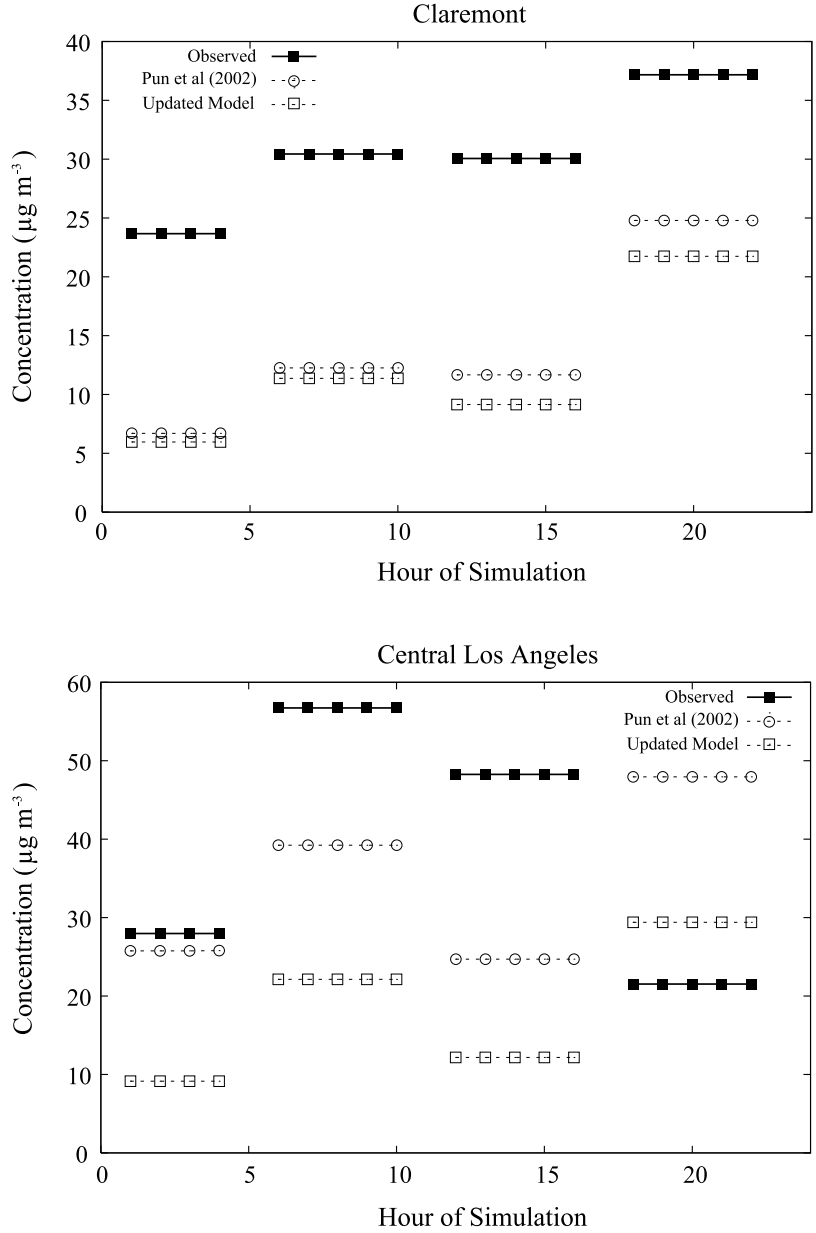

Figure 6. Comparison of simulated total organic aerosol concentrations for three-dimensional applications of SOA predictive models including that described by *Pun et al.* [2002] and the current model. Two locations in the SoCAB are shown for simulations of 8 September 1993.

procedure is likely to have the largest effect on predicted SOA because of the relatively high concentrations of aromatic precursors that lead to the formation of species UR26. In addition, by decreasing the general loss rate of nonreactive species in CACM, predicted SOA slightly increases. However, net decreases in SOA formation relative to prior three-dimensional applications of CACM and MPMPO are expected as a result of the changes described here that have been made to the individual modules.

[40] This fact is exemplified in Figure 6 in which output from a three-dimensional application of the current model is shown. The host model in this case is the California Institute of Technology (CIT) three-dimensional air quality model, and the simulations are performed for 8 September 1993 for the SoCAB. Details on the CIT model as well as relevant input parameters are discussed by *Griffin et al.* [2002b]. Simulation output is shown for central Los Angeles, an upwind site expected to be influenced heavily by primary emissions, and Claremont, a downwind site expected to be influenced by both primary and secondary processes. Results are shown compared to both observations and output from the original model of *Pun et al.* [2002], which is the precursor to MPMPO and therefore the model being discussed presently. It is clear that the modifications made to CACM and MPMPO result in a decrease in predicted SOA concentrations, as discussed above, because total organic aerosol concentrations decrease yet primary organic aerosol (POA) emissions are identical in the two scenarios. The upwind site appears to be affected to a greater degree by the changes made to CACM and MPMPO. Because of

the decreases in predicted organic aerosol concentrations, these changes are expected to have rectified some of the discrepancies identified by *Pun et al.* [2003] when comparing the original *Pun et al.* [2002] model to other modules used to predict SOA concentrations.

[41] It should also be noted that both models underpredict organic aerosol mass concentrations relative to observations. These underpredictions potentially are linked to underestimates of emissions of POA, lack of inclusion of particle phase chemistry that leads to increases in SOA yield, or other uncertainties in model parameters. It is also possible that parent VOCs not considered in the partitioning model lead to formation of ambient SOA in significant amounts. These include compounds that are traditionally ignored for SOA formation due to their small carbon number. However, low-carbon-number species such as isoprene are now thought to contribute to some SOA formation under certain atmospheric conditions [*Limbeck et al.*, 2003; *Claeys et al.*, 2004]. Sesquiterpenes are known to lead to SOA formation in high yield [*Griffin et al.*, 1999] but presently are not considered in CACM. Formation of SOA from other species currently not addressed in the model should be considered in future versions as improvements are achieved in our understanding of chemistry and speciation and rates of biogenic emissions.

[42] Despite the limitations discussed above, the model represents the state of the science in SOA predictive capabilities. It is based on fundamental reaction chemistry and thermodynamic properties of the participating species, which allows for application to numerous atmospheric scenarios. This framework also predicts the production of chemically speciated gas and aerosol phase products, which allows for apportionment of SOA to chemical characteristics of products (e.g., carboxylic acids) and sources of the parent VOCs (e.g., biogenic versus anthropogenic or aromatics versus long-chain alkanes).

[43] The current model attempts to account for particle phase chemistry (oligomer formation in a system devoid of POA and acid seed) to a very limited degree through adjustment of surrogate partitioning compound vapor pressures. It should also be noted that such a vapor pressure adjustment artificially accounts for any currently unknown gas phase processes that lead to nonvolatile oxidation products in small amounts. As additional kinetic and thermodynamic information becomes available regarding particle phase chemistry, it will be incorporated into the modules, particularly for the acid catalyzed reactions that lead to increases in SOA yield relative to nonacid conditions. There is also the potential for particle phase chemistry that leads to POA species becoming more favorable for absorption of SOA species (i.e., oxidation of pure hydrocarbons) and for association reactions between POA and SOA species. The ability to simulate individual product concentrations makes the module described here ideally amenable for simulating mixed inorganic-organic-water systems, the associated particle phase chemistry, and potential heterogeneous chemistry associated with POA once these phenomena are better understood. In this way, future versions of the model potentially will also allow for study of the effect that emissions of inorganic aerosol and gas phase species have on SOA formation.

[44] **Acknowledgments.** This work was performed, in part (RJG), under STAR Research Assistance agreement R831083 awarded by the U.S. Environmental Protection Agency (EPA) through a subcontract from the University of California at Davis. It has not been formally reviewed by EPA. The views expressed in this document are solely those of the authors, and EPA does not endorse any products or commercial services mentioned in this publication. This work was additionally supported, in part (DD), by the CAREER Award grant ATM-9985025 from the National Science Foundation. This work was also supported, in part (JHS), by the Electric Power Research Institute. Thank you also to William Allen and Satish Vutukuru for support in production of the figures in this manuscript and to anonymous reviewers for many helpful comments.

References

Asher, W. E., J. F. Pankow, G. B. Erdakos, and J. H. Seinfeld (2002), Estimating the vapor pressures of multi-functional oxygen-containing organic compounds using group contribution methods, *Atmos. Environ.*, *36*, 1483–1498.

Barsanti, K. C., and J. F. Pankow (2004), Thermodynamics of the formation of atmospheric organic particulate matter by accretion reactions—part 1: Aldehydes and ketones, *Atmos. Environ.*, *38*, 4371–4382.

Chung, S., and J. H. Seinfeld (2002), Global distribution and climate forcing of carbonaceous aerosols, *J. Geophys. Res.*, *107*(D19), 4407, doi:10.1029/2001JD001397.

Claeys, M., et al. (2004), Formation of secondary organic aerosols through photooxidation of isoprene, *Science*, *303*, 1173–1176.

Clegg, S. L., and J. H. Seinfeld (2004), Improvement of the Zdanovskii-Robinson-Stokes model for mixtures containing solutes of different charge types, *J. Phys. Chem.*, *108*, 1008–1017.

Clegg, S. L., J. H. Seinfeld, and P. Brimblecombe (2001), Thermodynamic modeling of aqueous aerosols containing electrolytes and dissolved organic compounds, *J. Aerosol Sci.*, *32*, 713–738.

Clegg, S. L., J. H. Seinfeld, and E. O. Edney (2003), Thermodynamic modelling of aqueous aerosols containing electrolytes and dissolved organic compounds. II. An extended Zdanovskii-Robinson-Stokes approach, *J. Aerosol Sci.*, *34*, 667–690.

Cocker, D. R., III, B. T. Mader, M. Kalberer, R. C. Flagan, and J. H. Seinfeld (2001), The effect of water on gas-particle partitioning of secondary organic aerosol: II. *m*-xylene and 1,3,5-trimethylbenzene photooxidation systems, *Atmos. Environ.*, *35*, 6073–6085.

Colville, C. J., and R. J. Griffin (2004), The roles of individual oxidants in secondary organic aerosol formation from Δ^3-carene—2: SOA formation and oxidant contribution, *Atmos. Environ.*, *38*, 4013–4023.

Czoschke, N. M., M. Jang, and R. M. Kamens (2003), Effect of acidic seed on biogenic secondary organic aerosol growth, *Atmos. Environ.*, *37*, 4287–4299.

Erdakos, G. B., W. E. Asher, J. H. Seinfeld, and J. F. Pankow (2005), Gas/particle partitioning of neutral and ionizing compounds to single and multi-phase aerosol particles. 3. Ionic–UNIFAC. 1: A method for predicting activity coefficients of neutral compounds in liquid aerosol particles containing organic compounds, dissolved inorganic salts, and water, *Atmos. Environ.*, in press.

Forstner, H. J. L., R. C. Flagan, and J. H. Seinfeld (1997), Secondary organic aerosol from photooxidation of aromatic hydrocarbons: Molecular composition, *Environ. Sci. Technol.*, *31*, 1345–1358.

Fredenslund, A., J. Gmehling, and P. Rasmussen (1977), *Vapor-Liquid Equilibrium Using UNIFAC*, Elsevier, New York.

Gao, S., N. L. Ng, M. Keywood, V. Varutbangkul, R. Bahreini, A. Nenes, J. He, K. Y. Yoo, R. C. Flagan, and J. H. Seinfeld (2004), Particle-phase acidity and oligomer formation in secondary organic aerosol, *Environ. Sci. Technol.*, *38*, 6582–6589.

Gard, E. E., et al. (1998), Direct observation of heterogeneous chemistry in the atmosphere, *Science*, *279*, 1184–1187.

Griffin, R. J., D. R. Cocker III, R. C. Flagan, and J. H. Seinfeld (1999), Organic aerosol formation from the oxidation of biogenic hydrocarbons, *J. Geophys. Res.*, *104*, 3555–3567.

Griffin, R. J., D. Dabdub, and J. H. Seinfeld (2002a), Secondary organic aerosol: 1. Atmospheric chemical mechanism for production of molecular constituents, *J. Geophys. Res.*, *107*(D17), 4332, doi:10.1029/2001JD000541.

Griffin, R. J., D. Dabdub, M. J. Kleeman, M. P. Fraser, G. R. Cass, and J. H. Seinfeld (2002b), Secondary organic aerosol: 3. Urban/regional scale model of size- and composition-resolved aerosols, *J. Geophys. Res.*, *107*(D17), 4334, doi:10.1029/2001JD000544.

Griffin, R. J., K. Nguyen, D. Dabdub, and J. H. Seinfeld (2003), A combined hydrophobic-hydrophilic module for predicting secondary organic aerosol formation, *J. Atmos. Chem.*, *44*, 171–190.

Hemming, B. L., and J. H. Seinfeld (2001), On the hygroscopic behavior of atmospheric organic aerosols, *Ind. Eng. Chem. Res.*, *40*, 4162–4171.

Hoffmann, T., J. R. Odum, F. Bowman, D. Collins, D. Klockow, R. C. Flagan, and J. H. Seinfeld (1997), Formation of organic aerosols from the oxidation of biogenic hydrocarbons, *J. Atmos. Chem.*, *26*, 189–222.

Iinuma, Y., O. Boge, T. Gnauk, and H. Herrmann (2004), Aerosol chamber study of the α-pinene/O_3 reaction: Influence of particle acidity on aerosol yields and products, *Atmos. Environ.*, *38*, 761–773.

Jacobson, M. Z. (1997), Development and application of a new air pollution modeling system, 3, Aerosol-phase simulations, *Atmos. Environ.*, *31*, 587–608.

Jang, M. S., and R. M. Kamens (2001), Atmospheric secondary aerosol formation by heterogeneous reactions of aldehydes in the presence of a sulfuric acid aerosol catalyst, *Environ. Sci. Technol.*, *35*, 4758–4766.

Jang, M. S., N. M. Czoschke, S. Lee, and R. M. Kamens (2002), Heterogeneous atmospheric aerosol production by acid-catalyzed particle-phase reactions, *Science*, *298*, 814–817.

Jaoui, M., and R. M. Kamens (2003), Mass balance of gaseous and particulate products from beta-pinene/O_3/air in absence of light and beta-pinene/NO_x/air in the presence of natural sunlight, *J. Atmos. Chem.*, *45*, 101–141.

Jenkin, M. E. (2004), Modeling the formation and composition of secondary organic aerosol from α- and β-pinene ozonolysis using MCM v3, *Atmos. Chem. Phys. Discuss.*, *4*, 2905–2948.

Jenkin, M. E., S. M. Saunders, V. Wagner, and M. J. Pilling (2003), Protocol for the development of the Master Chemical Mechanism, MCM v3 (part B): Tropospheric degradation of aromatic volatile organic compounds, *Atmos. Chem. Phys.*, *3*, 181–193.

Kalberer, M., et al. (2004), Identification of polymers as major components of atmospheric organic aerosols, *Science*, *303*, 1659–1662.

Kim, Y. P., J. H. Seinfeld, and P. Saxena (1993), Atmospheric gas-aerosol equilibrium I. Thermodynamic model, *Aerosol Sci. Technol.*, *19*, 157–181.

Lack, D. A., X. X. Tie, N. D. Bofinger, A. N. Wiegand, and S. Madronich (2004), Seasonal variability of secondary organic aerosol: A global modeling study, *J. Geophys. Res.*, *109*, D03203, doi:10.1029/2003JD003418.

Limbeck, A., M. Kulmala, and H. Puxbaum (2003), Secondary organic aerosol formation in the atmosphere via heterogeneous reaction of gaseous isoprene on acidic particles, *Geophys. Res. Lett.*, *30*(19), 1996, doi:10.1029/2003GL017738.

Lurmann, F. W., W. P. L. Carter, and L. A. Coyner (1987), A surrogate species chemical reaction mechanism for urban-scale air quality simulation models, *Rep. 600/3-87/014A*, U.S. Environ. Prot. Agency, Washington, D. C.

McRae, G. (1981), Mathematical modeling of photochemical air pollution, Ph.D. thesis, Calif. Inst. of Technol., Pasadena.

Meng, Z., J. H. Seinfeld, P. Saxena, and Y. P. Kim (1995), Atmospheric gas-aerosol equilibrium 4. Thermodynamics of carbonates, *Aerosol Sci. Technol.*, *23*, 131–154.

Meng, Z., D. Dabdub, and J. H. Seinfeld (1998), Size-resolved and chemically resolved model of atmospheric aerosol dynamics, *J. Geophys. Res.*, *103*, 3419–3435.

Ming, Y., and L. M. Russell (2002), Thermodynamic equilibrium of organic-electrolyte mixtures in aerosol particles, *AIChE J.*, *48*, 1331–1348.

Nguyen, K., and D. Dabdub (2002), Semi-Lagrangian flux scheme for the solution of the aerosol condensation/evaporation equation, *Aerosol Sci. Technol.*, *36*, 407–418.

Odum, J. R., T. Hoffmann, F. Bowman, D. Collins, R. C. Flagan, and J. H. Seinfeld (1996), Gas/particle partitioning and secondary organic aerosol yields, *Environ. Sci. Technol.*, *30*, 2580–2585.

Odum, J. R., T. P. W. Jungkamp, R. J. Griffin, R. C. Flagan, and J. H. Seinfeld (1997a), The atmospheric aerosol-forming potential of whole gasoline vapor, *Science*, *276*, 96–99.

Odum, J. R., T. P. W. Jungkamp, R. J. Griffin, H. J. L. Forstner, R. C. Flagan, and J. H. Seinfeld (1997b), Aromatics, reformulated gasoline, and atmospheric organic aerosol formation, *Environ. Sci. Technol.*, *31*, 1890–1897.

Pankow, J. F. (1994), An absorption model of gas/particle partitioning of organic compounds in the atmosphere, *Atmos. Environ.*, *28*, 185–188.

Pankow, J. F. (2003), Gas/particle partitioning of neutral and ionizing compounds to single and multi-phase aerosol particles. 1. Unified modeling framework, *Atmos. Environ.*, *37*, 3323–3333.

Pankow, J. F., J. H. Seinfeld, W. E. Asher, and G. B. Erdakos (2001), Modeling the formation of secondary organic aerosol: 1. The application of theoretical principles to measurements obtained in the α-pinene-, β-pinene-, sabinene-, Δ^3-carene-, and cyclohexene-ozone systems, *Environ. Sci. Technol.*, *35*, 1164–1172.

Pilinis, C. (1990), Derivation and numerical solution of the species mass-distribution equations for multicomponent particulate systems, *Atmos. Environ., Part A*, *24*, 1923–1928.

Pun, B. K., R. J. Griffin, C. Seigneur, and J. H. Seinfeld (2002), Secondary organic aerosol: 2. Thermodynamic model for gas/particle partitioning of molecular constituents, *J. Geophys. Res.*, *107*(D17), 4333, doi:10.1029/2001JD000542.

Pun, B. K., S.-Y. Wu, C. Seigneur, J. H. Seinfeld, R. J. Griffin, and S. N. Pandis (2003), Uncertainties in modeling secondary organic aerosols: Three-dimensional modeling studies in Nashville/western Tennessee, *Environ. Sci. Technol.*, *37*, 3647–3661.

Saunders, S. M., M. E. Jenkin, R. G. Derwent, and M. J. Pilling (2003), Protocol for the development of the Master Chemical Mechanism, MCM v3 (part A): Tropospheric degradation of nonaromatic volatile organic compounds, *Atmos. Chem. Phys.*, *3*, 161–180.

Seinfeld, J. H., and J. F. Pankow (2003), Organic atmospheric particulate material, *Annu. Rev. Phys. Chem.*, *54*, 121–140.

Seinfeld, J. H., G. B. Erdakos, W. E. Asher, and J. F. Pankow (2001), Modeling the formation of secondary organic aerosol: 2. The predicted effects of relative humidity on aerosol formation in the α-pinene-, β-pinene-, sabinene-, Δ^3-carene-, and cyclohexene-ozone systems, *Environ. Sci. Technol.*, *35*, 1806–1817.

Sheehan, P. E., and F. M. Bowman (2001), Estimated effects of temperature on secondary organic aerosol concentrations, *Environ. Sci. Technol.*, *35*, 1806–1817.

Takekawa, H., H. Minoura, and S. Yamazaki (2003), Temperature dependence of secondary organic aerosol formation by photo-oxidation of hydrocarbons, *Atmos. Environ.*, *37*, 3413–3424.

Tolocka, M. P., M. Jang, J. M. Ginter, F. J. Cox, R. M. Kamens, and M. V. Johnston (2004), Formation of oligomers in secondary organic aerosol, *Environ. Sci. Technol.*, *38*, 1428–1434.

Tsigaridis, K., and M. Kanakidou (2003), Global modelling of secondary organic aerosol in the troposphere, *Atmos. Chem. Phys.*, *3*, 1849–1869.

Yu, J., D. R. Cocker III, R. J. Griffin, R. C. Flagan, and J. H. Seinfeld (1999), Gas-phase ozone oxidation of monoterpenes: Gaseous and particulate products, *J. Atmos. Chem.*, *34*, 207–258.

Zhang, Y., C. Seigneur, J. H. Seinfeld, M. Jacobson, S. L. Clegg, and F. S. Binkowski (2000), A comparative review of inorganic aerosol thermodynamic modules: Similarities, differences, and their likely causes, *Atmos. Environ.*, *34*, 117–137.

D. Dabdub, Department of Mechanical and Aerospace Engineering, University of California, Irvine, CA 92697, USA.

R. J. Griffin, Institute for the Study of Earth, Oceans, and Space, University of New Hampshire, 39 College Road, Durham, NH 03824, USA. (rjg@gust.sr.unh.edu)

J. H. Seinfeld, Departments of Chemical Engineering and Environmental Science and Engineering, California Institute of Technology, Pasadena, CA 91125, USA.